JSEE Vol. 27, No. 2, 2025 DOI: 10.48303/jsee.2024.2034254.1108

*Research Paper*

# Tectonic Model-Based Critique on Conventional Seismic Hazard Evaluations; Implications for the Role of the South Caspian Basin on Seismicity of Northern Iran

***Zaman Malekzade***

Assistant Professor, Department of Geology, Payam-e Noor University, Tehran, Iran, z_malekzadeh@pnu.ac.ir

**Received:** 30/06/2024
**Revised:** 15/11/2024
**Accepted:** 30/11/2024

## ABSTRACT

Reconnaissance, definition, mapping, and mechanism(s) of the earthquake sources are the preliminary earthquake hazard analysis strategies. Heterogeneity of the crust, change in stress, and diffuse and distributed nature of the present-day continental deformation are the features that may influence the seismic sources, which, in turn, determine the seismic hazard assessment policy. The mechanisms and geometry of the sources potentially relate to the physics of the crust and then the magnitude, duration, and depth of generated earthquakes, etc. Tectonics, on the other hand, deals with recovering the stress state, and consequent deformations represented by geostructures, including the faults and folds. Therefore, the tectonic investigations and modeling may lead to better definitions and characteristics of the seismic sources. This study introduces a new approach to defining earthquake sources and segmentation, providing a practical guideline for evaluating earthquake occurrences. This evaluation model is supported by geological evidence that forms a crucial component of Probabilistic Seismic Hazard Assessment (PSHA) and Deterministic Seismic Hazard Analysis (DSHA) programs. The tectonic model's key output is the segmentation of fault zones responsible for earthquakes, some of which could be blind faults or faults yet to be identified as active faults. These regions might be regarded as seismic areas in conventional seismic evaluations. The study recommends distinguishing between seismic hazard and seismic risk maps in regions where the potential for seismic activity is the same, but the population densities differ.

**Keywords:**
Tectonic model; Seismicity; Zipper tectonics; Segmentation

How to cite the article:
Malekzade, Z. (2025). Tectonic model-based critique on conventional seismic hazard evaluations; implications for the role of the South Caspian Basin on seismicity of northern Iran. *Journal of Seismology and Earthquake Engineering*, *27*(2), 1-14. doi: 10.48303/jsee.2024.2034254.1108

## 1. Introduction

So far, tectonics has been used for mapping or reconnaissance of active faults as a primary source of earthquakes. Geomorphic features, fault kinematic measurements, paleoseismology, geodetic data, image processing, and seismicity allow geologists to consider the seismic activity of an area and determine whether it is potentially seismogenic. The next steps for seismic evaluation involve seismic hazard assessments using deterministic and probabilistic methodologies. Both assessment approaches require a precise definition of active faults as seismic sources, which is crucial for evaluating seismic hazards in a study area. However, defining active faults can be challenging in seismic evaluations, especially when faults are obscured by Neogene deposits or when faults behave as blind faults and have different kinematics and geometry in surface and depth, potentially leading to erroneous conclusions in seismic hazard assessments. For instance, the M = 6.6 Bam earthquake on December 26, 2003, which resulted in a death toll exceeding 50,000 (Jackson et al., 2006; Talebian et al., 2004), and the Rudbar Mw 7.3 earthquake on June 20, 1990, causing nearly 40,000 fatalities, occurred on previously unmapped faults (Berberian & Walker, 2010). This underscores the importance of accurately defining earthquake sources as the initial step in seismic hazard evaluations, emphasizing the significance of tectonic modeling. Tectonic modeling involves introducing a methodology to represent fault patterns rather than focusing solely on individual active faults (Malekzade & Bellier, 2024).

Geologists, therefore, need to develop stress maps to understand the stress state in the upper crust, relying on fault kinematic measurements and geophysical studies at a lithospheric level to elucidate fault patterns. This study aims to introduce a system of strike-slip faults that have contributed to crustal deformation in northern Iran, particularly during the Holocene epoch (see Figure 1), which is explained as zipper tectonics in this study. In addition, the article addresses the effects of the suture zones on the distribution of active strike-slip faults as a considerable seismic source in northern Iran.

## 2. Tectonic Setting

The Iranian segment of the Alpine-Himalayan chain has been witnessing collisional tectonic events since the Middle-Late Tertiary period. This collision resulted in the separation of the South Caspian Basin (SCB) from the Black Sea (e.g., Chu et al., 2021), similar to other remnants of the Paleo-Tethys Ocean. Following the Neo-Tethys slab break-off,

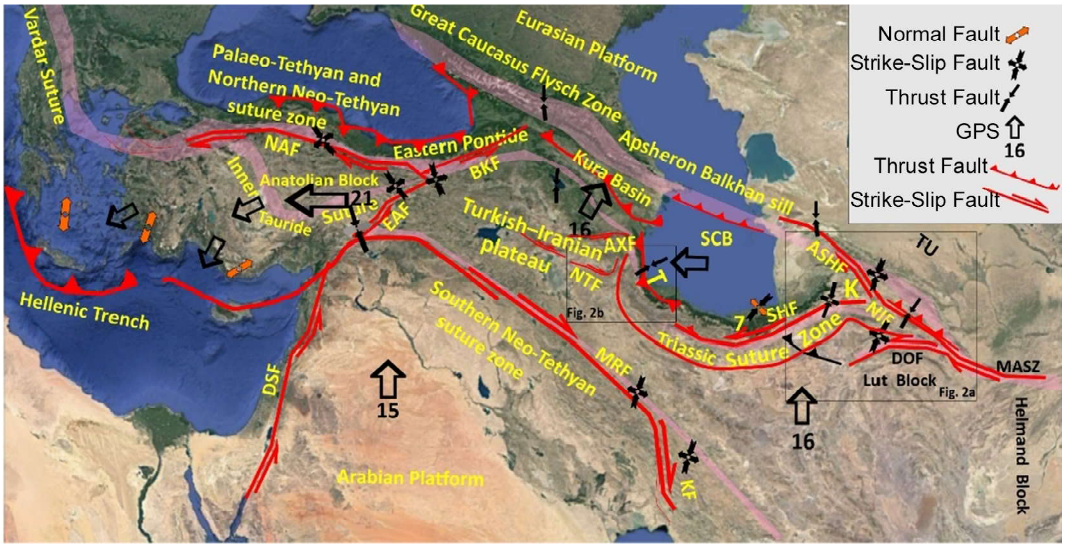


**Figure 1.** A simplified tectonic map of the west central part of the Alp-Himalaya orogenic belt. The stress tensors were adapted from Avagyan et al. (2005) along the Caucasus, Faccenna et al. (2006) along the north- and east Anatolian Faults, Shabanian et al. (2010) in Kopeh Dagh, Javidfakhr et al. (2011a) along the eastern Alborz and southwestern Kopeh Dagh, Farbod et al. (2011) along the Doruneh Fault. Abbreviations are EAF = East Anatolian Fault, NAF = North Anatolian Fault, HT = Hellenic Trench, TAL = Talesh, TIP=Turkey-Iranian Plateau, MZRF = Main Zagros Reverse Fault, KZF = Kazerun Fault, DSF = Dead Sea Fault, K = Kopeh Dagh, SHF=Shahrud Fault, NIF = Nishabur Fault, DOF = , MASZ = Main Afghanistan Suture Zone, ASHF= Ashghabat Fault, TU = Turan Plate.

the uplift of the Turkish-Iranian Plateau, the propagation of strike-slip faults, and the westward movement of the Anatolian Plateau in response to the retreat of the Hellenic trench have been identified as key hierarchical tectonic events after the collision. Figure (1) illustrates the current tectonic configuration of the study area, where the Arabian plate has pushed into the southern margin of Eurasia. The image showcases the lateral continental movement of Anatolia through the gradual reworking of preexisting conjugate shear zones like the North Anatolian Fault (NAF) and the East Anatolian Fault (EAF). In this framework, various crustal blocks (e.g., Afghan, Lut, SCB, and Anatolia blocks) are separated by deformation zones, including regions such as eastern Iran, Binalud, Kopeh Dagh, Alborz, Talesh, and the Turkish-Iranian Plateau from east to west, respectively. These separated blocks have potentially migrated westward during and subsequent to the north-south collision events involving Arabia, India, and Eurasia, facilitated by suture zones within time frames of less than three million years as demonstrated in Figure (1).

Considering a transpressional tectonic regime on NE-striking faults (say 210°) in eastern Alborz or western Kopeh Dagh (e.g. Javidfakhr et al., 2011a; Shabanian et al., 2010) the azimuth of the motion of the SCB is ~210° to 300° relative to central Iran and Eurasia (Jackson et al., 2002). In the course of its movement northwestwards (300°), the SCB subducts beneath the northern Caspian, resulting in a second tectonic force in addition to the existing force induced by Arabian plate convergence (Masson et al., 2006; 2007), and providing a free boundary, dilatation zones, or space for escape of the crustal fragments. The strike-parallel component (210°) drives the SCB to the SW, leading it to subduct beneath the Talesh (e.g., Azad et al., 2019). The left strike-slip faulting within Alborz and the NE-trending faults in Kopeh Dagh are related to a younger event (Ritz et al., 2006; Hessami, 2020). The onset of left-slip faulting in Alborz has been assigned to the block rotation that is attributed to a trade-off in strain between collision along Kopeh Dagh and subduction in the Kura basin and Upsheron-Balkhan sill (Malekzade, 2018). This kind of rotation is not limited to the clockwise rotation of the SCB. It, however, include a deformation zone containing Alborz, Talesh, and northern part of the central Iran (Malekzade, 2018). In the context of the deforming regions, the rotation influences the basement faulted blocks in response to the inversion of normal faults generated by sets of releasing bents inherited since Paleozoic and Mesozoic right lateral strike-slip faulting (e.g., Hessami, 2020). According to the model proposed by Hollingsworth et al. (2006) for NE Iran, the north-to-south shortening started from the east and has extended to the west by anticlockwise rotation of a series of right-slip faulted blocks as a result of which the western Kopeh Dagh is forced to the west. The shortening started c.a. 24 Ma in eastern Kopeh Dagh, and ~5 Ma in western Kopeh Dagh (Tavakoli, 2007). The increase in GPS velocity vector confirms the westward increase in the shortening rate (Tavakoli, 2007; Mousavi et al., 2013) and/or westward extrusion of the SCB (Figure 2a). Figure (2b) may alternatively imply the westward extrusion of crustal wedges accompanying the SCB.

## 3. Methodology

This study uses kinematic approaches to investigate seismic activities in northern Iran. The primary data sources include fault slip measurements and slip vectors derived from focal mechanisms. Additionally, historical and instrumental earthquake records from websites such as http://www.iiees.ac.ir/en/eqcatalog/ and http://irsc.ut.ac.ir/bulletin.php are incorporated. GPS data obtained from GPS campaigns are also referenced in the study. Kinematic analyses play a crucial role and are extensively utilized in this research to understand the seismic behavior in the region. Carey-Gailhardis and Mercier (1987) presented a quantitative inversion of the fault slip and/or focal mechanisms. Two assumptions are implicit in the procedure of inversion: (1) the slip, which is represented by the slip vector corresponding to the rake in earthquake focal mechanisms and striations on the fault planes, occurred along with the resolved shear stress ($\tau$), and (2) faults are pre-existing planes. A mean best-fitting deviatoric stress tensor is computed by minimizing the angular deviation between a predicted slip vector (maximum shear, $\tau$) and the observed

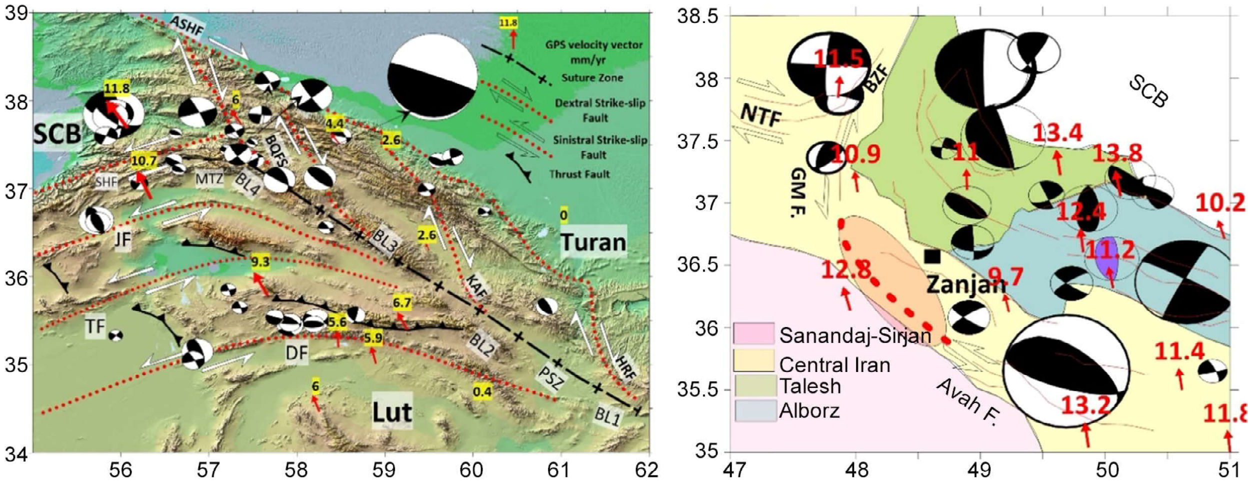


(a) (b)

**Figure 2.** Two seismotectonic maps of northern Iran. (a) Northeastern Iran: indicating dextral closing zipper Y-shape fault pattern making a fish-bone structure composed from NW- and SW-trending right- and left lateral strike-slip faults, respectively, and suture zone playing backbone of the structure (superimposed on extracted segment). Arrows are GPS (Tavakoli, 2007). The GPS show increasing values toward NW, confirming westward expulsion of SCB. Focal mechanisms (Farbod et al., 2011; Javidfakhr et al., 2011b; Su et al., 2018). (b) A seismotectonic map of northwestern Iran where North Tabriz Fault (NTF) dextral strike-slip fault and Gamachay (GM. F) left lateral strike-slip conjugated faults join to the Bozghush (BZF) left-slip fault as the extracted segment of a left closing zipper. The distance between Gamachay and Avaj Faults in south of Zanjan city make a seismic gap along which no faults are mapped.

slip vector (s) deduced from either a set of fault-slip vectors or a focal mechanism (Carey & Brunier, 1974; Carey, 1979). As mentioned above, in the case of fault-slip data, we assume that each striation represents an ideal focal plane in a seismic event. The results are the trend and plunge of the principal axes of the mean deviatoric stress tensor ($\sigma_1 \geq \sigma_2 \geq \sigma_3$), the magnitude of each principal stress, and a "stress ratio" $R=(\sigma_2-\sigma_1)/(\sigma_3-\sigma_1)$ (Tables 1 and 2). Figure (3) demonstrates the details of the kinematics analyses results. Figure (4) shows the direction of compression (in the case of strike-slip and thrust faults) deduced by the inversion of fault slips. In case of normal faults, the arrows in Figure (3) show the direction of minimum stress axes (extension). To have a good coverage of fault kinematics information, this study utilizes the outsource data that is presented in Table (3).

## 4. Structural Descriptions

In the tectonic model proposed by this study, the South Caspian Basin (SCB) plays a crucial role in the tectonic and structural evolution of the Iranian plateau. The tectonic transition from collision in Kopeh Dagh to subduction along the Apsheron-Balkhan Sill has resulted in the migration of the SCB and its surrounding crustal blocks from east to west (Malekzade, 2018; Hessami, 2020).

**Table 1.** Stress inversion results for earthquake focal mechanisms. The principal deviatoric stress axes $\sigma_1 \geq \sigma_2 \geq \sigma_3$ are specified by their trends measured from the north, and their plunge. TR represents the tectonic regime in which SS= strike-slip fault, T= Thrust fault, and N = Normal fault (if any), $R = (\sigma_2-\sigma_1)/(\sigma_3-\sigma_1)$, the "stress ratio" of the deviatoric stress tensor.

| ID | Reference | Location | Azimuth of | | | R | Plunge of | | | TR |
|---|---|---|---|---|---|---|---|---|---|---|
| | | | $\sigma_1$ | $\sigma_2$ | $\sigma_3$ | | $\sigma_1$ | $\sigma_2$ | $\sigma_3$ | |
| 1 | Jackson et al., 2002 | Caucasus | 190 | 100 | 282 | 0.3 | 0 | 11 | 78 | T |
| 2 | Nemati et al., 2011 | NW of Iran | 340 | 71 | 184 | 0.7 | 6 | 2 | 83 | T |
| 3 | Jackson et al., 2002 | Talesh | 71 | 161 | 308 | 0.4 | 4 | 6 | 83 | T |
| 4 | Jackson et al., 2002 | Apsheron Balkhan | 164 | 73 | 305 | 0.7 | 4 | 4 | 84 | T |
| 5 | Tatar & Hatzfeld, 2009 | Rudbar | 239 | 149 | 33 | 0.2 | 9 | 4 | 80 | T |
| 6 | Nemati et al., 2011 | Eastern Alborz | 18 | 108 | 267 | 0.9 | 3 | 10 | 78 | T |
| 7 | Jackson et al., 2002 | Central Alborz | 66 | 158 | 335 | 0.8 | 1 | 64 | 25 | SS |
| 8 | Jackson et al., 2002 | Kopeh Dagh | 222 | 130 | 4 | 0.6 | 14 | 10 | 72 | T |
| 9 | Su et al., 2018 | Mashhad | 35 | 126 | 282 | 0.5 | 5 | 11 | 77 | T |

**Table 2.** Results of the fault kinematic analyses produced in this study (see text for more information). $\sigma_1$, $\sigma_2$, and $\sigma_3$ are maximum, medium and minimum stress axes of a stress tensor. The R-values marked by a star were generated by fixed inversion presented by Bellier and Zoback (1995).

| Site | Longitude | Latitude | $\sigma_1$ | $\sigma_2$ | $\sigma_3$ | R | TR | Age (Rock Type) |
|---|---|---|---|---|---|---|---|---|
| 1 | 48.06656 | 36.29813 | 65/084 | 10/330 | 21/236 | 0.7 | N | Neogene |
| 2 | 48.40187 | 37.68582 | 68/223 | 19/021 | 07/114 | 0.5 | N | Eocene |
| 3 | 48.7555 | 37.53847 | 07/063 | 08/154 | 79/291 | 1 | T | Jurassic |
| 4 | 48.79 | 36.733 | 11/036 | 73/172 | 11/304 | 0.9 | SS | Eocene |
| 5 | 48.978 | 36.81 | 89/100 | 00/267 | 00/357 | * | N | Miocene |
| 7 | 49.624 | 36.67 | 00/072 | 00/162 | 89/341 | * | T | Jurassic |
| 8 | 50.209 | 36.387 | 00/205 | 06/115 | 83/295 | 1 | T | Eocene |
| 10 | 50.668 | 36.119 | 17/058 | 03/327 | 71/227 | 0.4 | T | Eocene |
| 11 | 50.741 | 36.379 | 00/088 | 00/178 | 89/324 | * | T | Mesozoic |
| 12 | 50.916 | 36.174 | 10/240 | 46/341 | 41/141 | 0.5 | SS | Mesozoic |
| 13 | 52.76 | 35.753 | 89/152 | 00/334 | 00/244 | * | N | Pleistocene |
| 14 | 51.57 | 35.83 | 06/219 | 72/109 | 16/311 | 1 | SS | Eocene |
| 15 | 51.966 | 35.78 | 24/046 | 63/244 | 07/139 | 0.3 | SS | Mesozoic |
| 16 | 52.336 | 36.136 | 00/048 | 00/138 | 89/315 | 0.2 | T | Paleozoic |
| 17 | 52.4 | 35.62 | 00/63 | 86/153 | 03/333 | 0.2 | SS | Quaternary |
| 18 | 53.277 | 35.837 | 16/017 | 04/109 | 72/214 | 0.6 | T | Cambrian |
| 19 | 53.37114 | 36.30691 | 13/231 | 12/325 | 70/096 | 0.03 | T | Cretaceous |
| 20 | 53.687 | 36.04 | 81/348 | 05/124 | 05/214 | 0.5 | N | Mesozoic (Limestone) |
| 21 | 53.854 | 36.3491 | 81/111 | 00/202 | 8/292 | 0.6 | N | Mesozoic (Limestone) |
| 22 | 54.51 | 36.37 | 03/242 | 04/332 | 83/112 | 0.1 | T | Plio-Pleistocene |
| 23 | 54.6383 | 36.4829 | 13/067 | 05/158 | 07/269 | 0.52 | T | Quaternary |
| 24 | 55.4132 | 36.36451 | 01/195 | 79/292 | 10/104 | 0.45 | SS | Eocene |
| 25 | 55.93 | 36.11 | 00/213 | 00/123 | 89/306 | * | T | Eocene |
| 26 | 57.981 | 35.37245 | 00/064 | 76/156 | 13/334 | 0.2 | SS | Cambrian |
| 28 | 58.715 | 35.288 | 14/054 | 42/311 | 44/159 | 0.3 | SS | Paleozoic |
| 29 | 59.4184 | 35.909 | 11/010 | 31/273 | 55/118 | 0.7 | SS | Quaternary |
| 30 | 58.019 | 35.4659 | 00/239 | 74/331 | 15/149 | 0.8 | SS | Cretaceous |
| 31 | 59.199 | 35.2209 | 00/071 | 00/161 | 90/333 | * | T | Oligocene |

**Table 3.** he external data used by this article to complete the information on fault kinematics. The symbols and abbreviations are the same as in Table (2).

| Name | Site | Longitude | Latitude | Modern Stress | | | R | Paleostress | | | | | TR | Reference |
|---|---|---|---|---|---|---|---|---|---|---|---|---|---|---|
| | | | | $\sigma_1$ | $\sigma_2$ | $\sigma_3$ | | TR | $\sigma_1$ | $\sigma_2$ | $\sigma_3$ | R | | |
| 1 | 3 | 58.095 | 37.686 | 4/218 | 5/309 | 84/92 | 0.852 | T | 4/162 | 36/255 | 54/66 | 0.887 | T | Shabanian et al., 2010 |
| 2 | 5 | 58.007 | 37.487 | 4/19 | 4/109 | 84/240 | 0.557 | T | 9/140 | 66/254 | 29/45 | 0.816 | SS | “ |
| 3 | 19 | 58.515 | 36.724 | 11/35 | 77/187 | 6/303 | 0.457 | SS | 15/318 | 39/60 | 47/212 | 0.881 | T | “ |
| 4 | 20 | 58.627 | 36.383 | 1/210 | 87/101 | 3/300 | 0.708 | SS | 10/141 | 17/48 | 70/261 | 0.158 | T | “ |
| 5 | 27 | 59.542 | 35.857 | 12/28 | 12/121 | 72/255 | 0.858 | T | 4/143 | 79/33 | 10/233 | 0.952 | SS | “ |
| 6 | 29 | 57.006 | 37.571 | 02/015 | 21/106 | 69/279 | 0.533 | T | 5/165 | 25/275 | 64/064 | 0.429 | T | “ |
| 7 | 1 | 58.466 | 35.287 | 06/038 | 56/136 | 33/304 | 0.95 | SS | 0/140 | 0/52 | 90/322 | 0.57 | T | Farbod et al., 2011 |
| 8 | 2 | 58.591 | 35.28 | 02/038 | 19/308 | 71/135 | 0.86 | T | 13/129 | 8/37 | 75/278 | 0.78 | T | “ |
| 9 | 3 | 58.773 | 35.27 | 02/067 | 58/198 | 21/328 | 0.43 | SS | 9/331 | 79/206 | 6/82 | 0.61 | SS | “ |
| 10 | 4 | 58.849 | 35.264 | 03/060 | 65/157 | 25/328 | 0.81 | SS | 2/31 | 78/131 | 12/400 | - | SS | “ |
| 11 | 5 | 58.335 | 35.294 | 02/031 | 78/131 | 12/040 | 0.23 | SS | - | - | - | - | - | “ |
| 12 | 40 | 56.86 | 37.35 | 22/226 | 68/39 | 2/135 | 0.47 | SS | 13/272 | 75/122 | 7/004 | 0.71 | SS | Javidfakhr et al. 2011(a) |
| 13 | 47 | 56.4 | 37.73 | 09/210 | 42/111 | 45/310 | 0.98 | T | 2/313 | 24/44 | 66/218 | 0.46 | T | “ |
| 14 | 35 | 56.44 | 37.23 | 13/233 | 75/28 | 6/142 | 0.99 | SS | 15/184 | 72/332 | 9/92 | - | SS | “ |
| 15 | 27 | 55.86 | 36.97 | 09/281 | 14/13 | 73/159 | 0.76 | T | 3/198 | 19/290 | 70/100 | 0.83 | T | “ |
| 16 | 48 | 56.33 | 37.74 | 03/198 | 19/290 | 70/100 | 0.62 | T | 1/325 | 19/55 | 71/233 | 1 | T | “ |

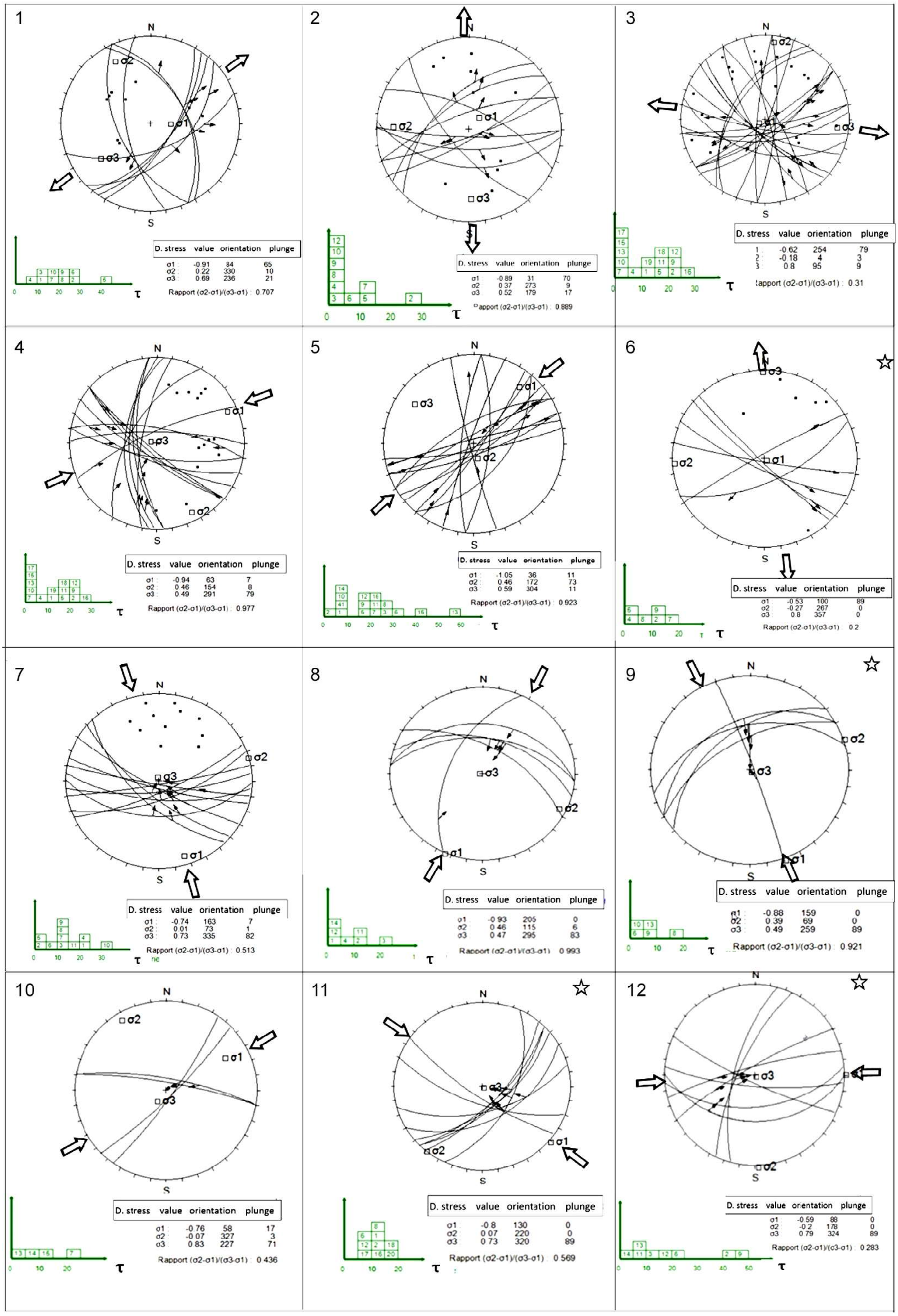

**Figure 3.** The fault slip inversion results are presented using equal angle, lower hemisphere stereonets. Arrows on the fault planes indicate the kinematics, with arrows converging toward the center of the hemisphere representing compression and arrows diverging from the center indicating extension. Site numbers, shown in black quadrangles, are illustrated in Figure (4a). The tensors, labeled with the names of the authors, represent the results of slip vectors from earthquakes. Histograms located in the bottom left of each hemisphere show the angular deviation (in degrees) between the striations and the computed shear stress for each fault. In the table at the bottom right of each hemisphere, the stress ratio is given by R = ($\sigma_2 \geq \sigma_1$) / ($\sigma_3 \geq \sigma_1$). The magnitude of each principal axis, along with the strike and dip of the axes, is provided in the first, second, and third rows of the table, respectively.

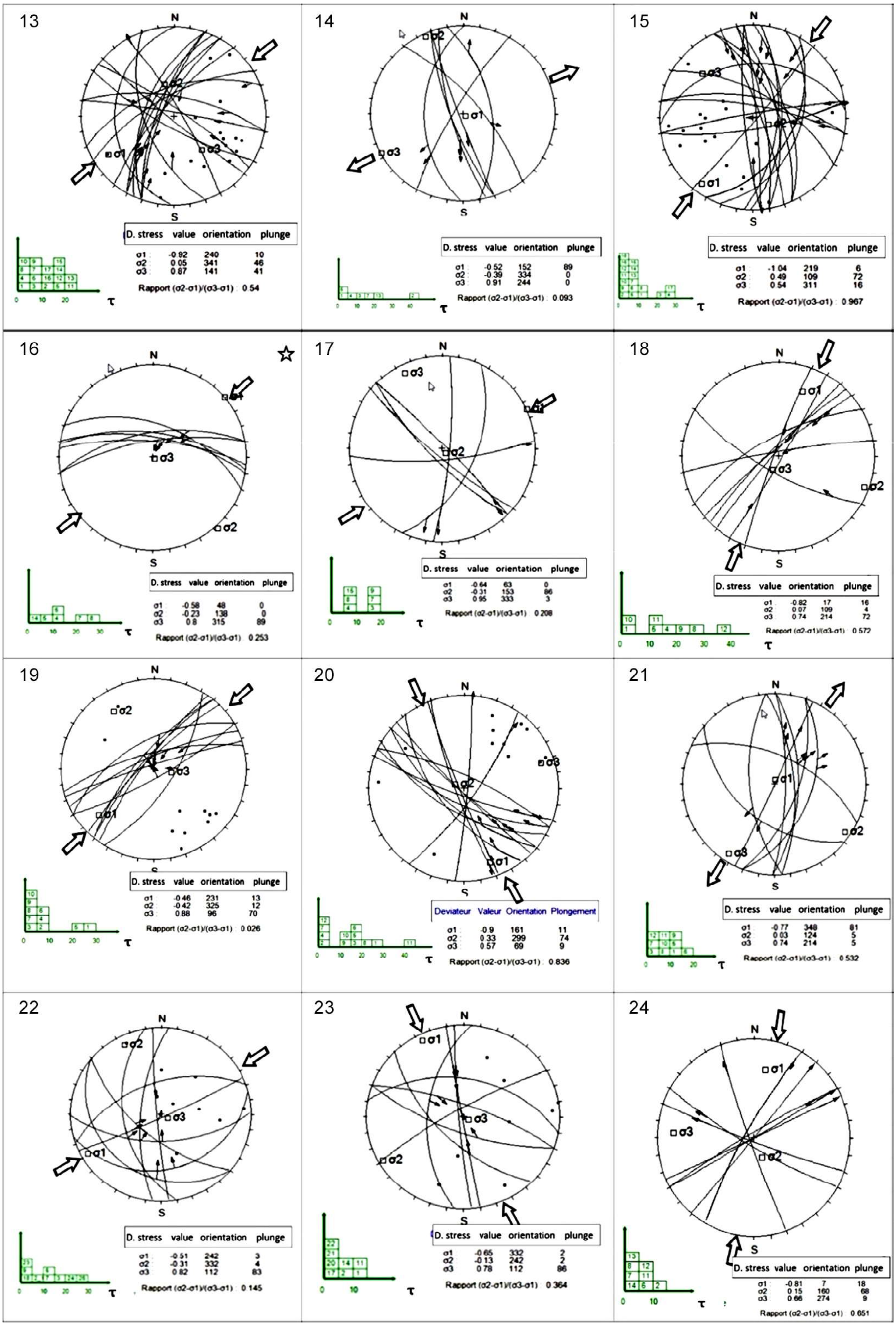

**Figure 3.** Continue.

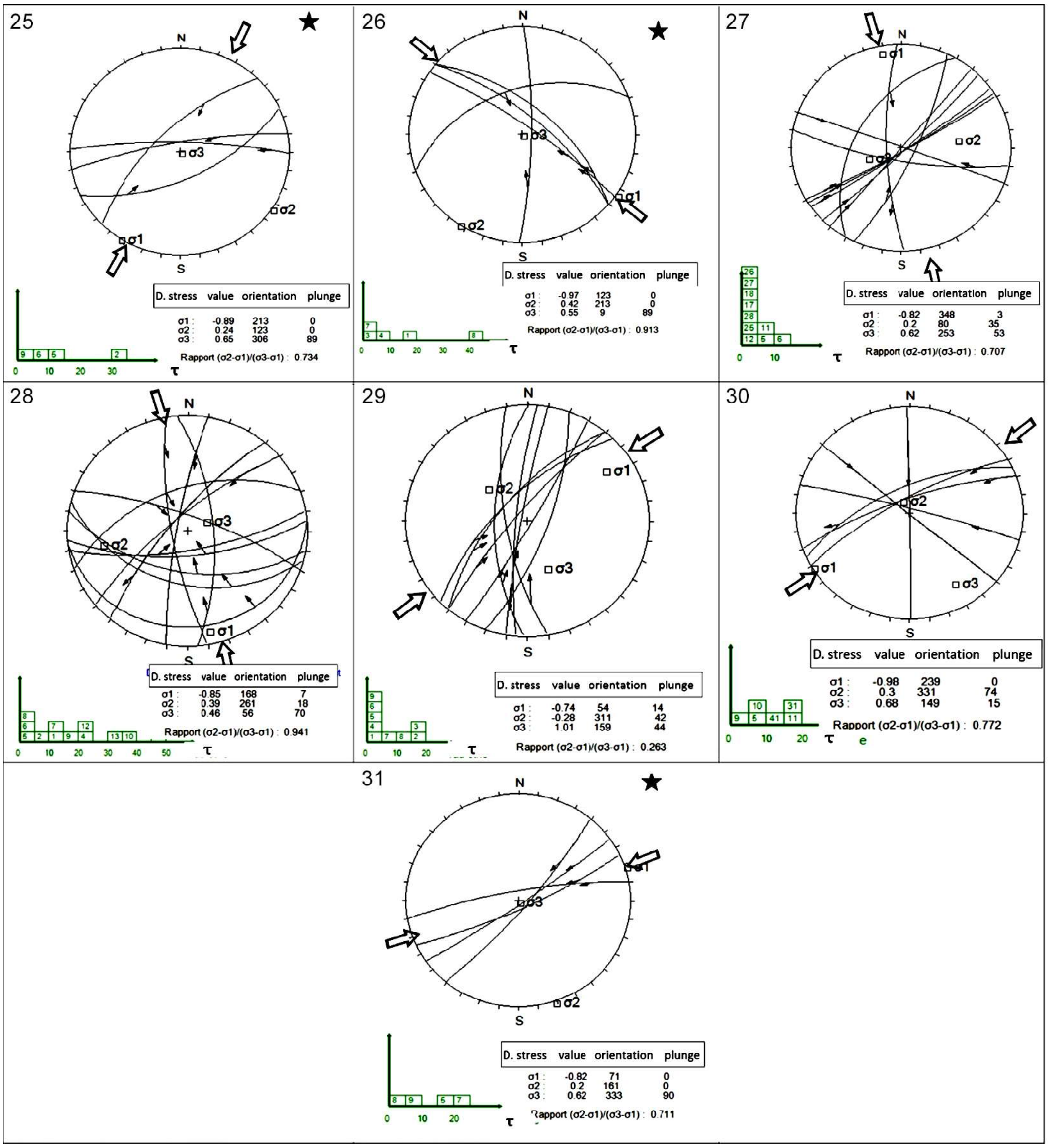


**Figure 3.** Continue.

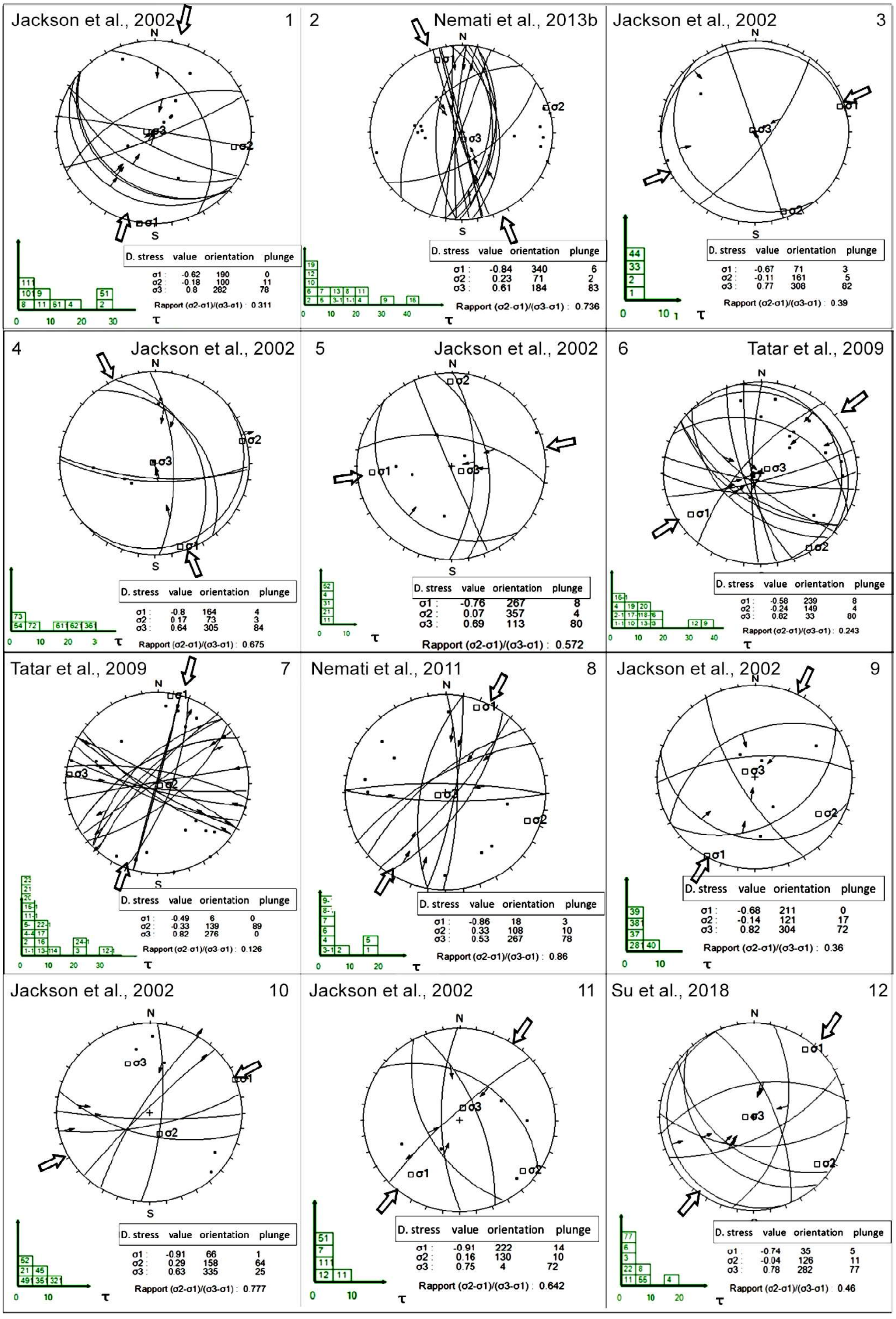


**Figure 3.** Continue.

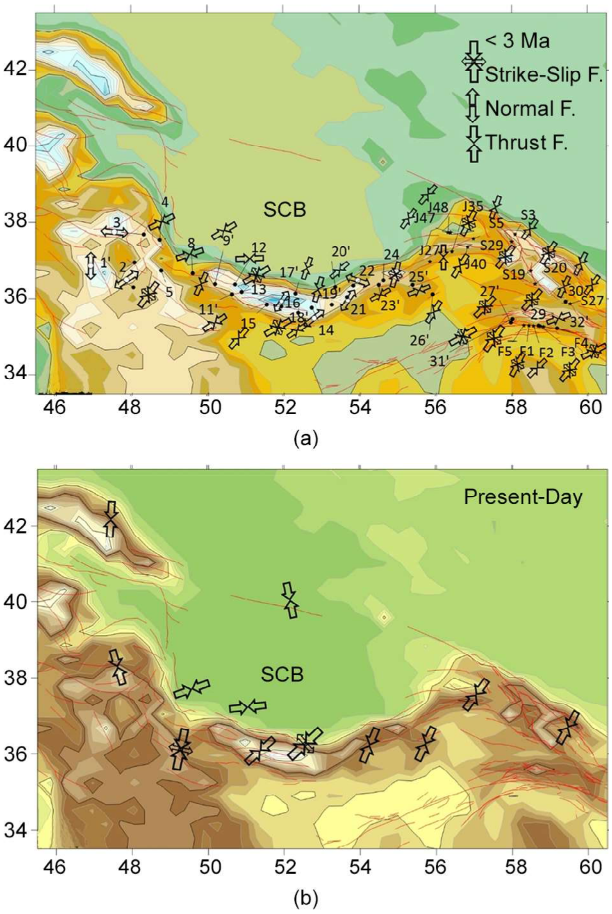


**Figure 4.** (a) The modern stress state map of the study area defines the axes of stress, with $\sigma_1$ (the maximum horizontal stress axis) related to strike-slip and thrust faults, and $\sigma_3$ (the minimum horizontal stress or extension axis) associated with normal faults. The data for this map are derived from the inversion of fault slip data, as shown in Figure (3) and Tables (1) and (2) from this study, along with Table (3) from other authors. The symbols marked with numbers correspond to the site numbers in Table (1). Symbols labeled with S, J, and F refer to data adapted from Shabanian et al. (2010), Javidfakhr et al. (2011a), and Farbod et al. (2011), respectively. Additionally, part b of the stress state map is deduced from the inversion of focal mechanisms presented in Figure (3).

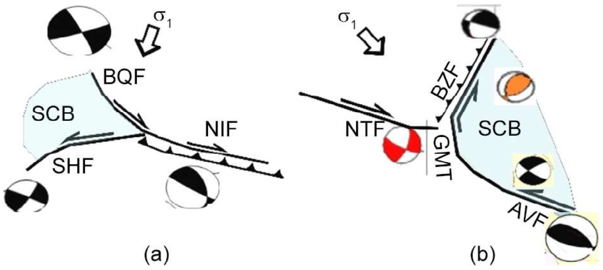


**Figure 5.** The geometry of a) dextral closing zipper; a proposed model for northeastern Iran. Focal are after Jackson et al. (2002): b) stretching junction model suggesting an ongoing tectonic activity in northwestern Iran. Focal adapted from Afra et al., 2017). The $\sigma_1$ are maximum horizontal stress axes deduced from Table (1). NIF (Nishabor Fault) and BZF are extracted segments where the conjugated strike-slip faults (BQF and SHF in northeastern Iran, and NTF and GMF in northwestern Iran) join to a transpressional faults (BZF and NIF) in a Y-shape configuration.

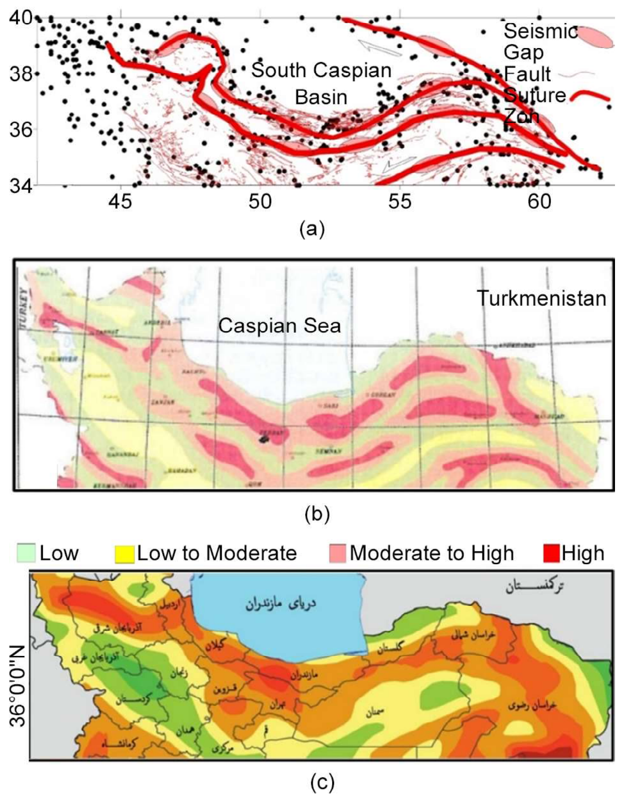


**Figure 6.** (a) The seismotectonic map displays suture zones overlaid with historically and instrumentally recorded seismic events. The ellipses indicate seismic gaps within the suture zones, which are proposed as segments that may experience future seismic activity, rather than being considered aseismic or less threatening areas. (b) The seismic hazard map presented by Tavakoli and Ghafory-Ashtiany (1999) is shown. (c) An up-dated seismic hazard map released by Zare (2017) is also in-cluded. As indicated in Figures (3b) and (3c), the high and very high seismic hazard zones correspond to what is referred to as suture zones in this article.

According to the model presented by this study, the SCB acts as a rigid body, while a conjugated sinistral and dextral strike-slip fault system is present (Figure 5). Due to the rigidity of the SCB, it moves westward in conjunction with a progressing dextral closing zipper mode behind it (Figures 3a and 4a). This zipper structure consists of two branches that converge into a compressional zone known as the extraction fault, where the fault kinematics shift from strike-slip to a transpressional regime (Figure 5). Figures (2a) and (5a) illustrate a simplified ye realistic representation of the dextral closing zipper in northeastern Iran. Moving westward, the northwestern Iranian plateau, which was already experiencing compression from the Arabia-Eurasia collision, now faces an additional westward tectonic force from the SCB (Azad et al., 2019). The westward advance of the SCB results in the formation of a conjugated fault system comprising NW- and NNE-trending sinistral faults and NW-trending dextral strike-slip faults within a system of stretching junction zippers (Figure 2b and Figure 5b).

## 5. Results

According to the fault kinematic measurements supported by the focal mechanisms, the modern far-field stress state along the southern Eurasia boundary, focusing on the Caucasus and Kopeh Dagh collision zones, is approximately oriented N (Malekzade, 2018; Lyberis & Manby, 1999). However, there is a shift in the stress distribution within the deformation zones inside the Iranian plateau (Malekzade, 2018; Shabanian et al., 2010; Javidfakhr et al., 2011a). The trend of compression is approximately NNE-NE in northeastern Iran (Figure 1 & Figure 5), and approximately NW in northwestern Iran (Figure 3). These stress states are influenced by the motion of the Iranian plateau relative to Eurasia and the westward escape of the South Caspian Basin.

The kinematic arguments presented by this study (Figure 4, Tables 1 and 2) and the preexisting data from other studies (Table 3) also indicate that the suture zone(s) play a crucial role in influencing the stress state and fault kinematics. This draws attention to how the motion of rigid plates to the west could deform the surrounding plates (NE and NW central Iran in Figure 1), altering the geometry of the shear (suture) zones and, consequently, leading to the formation of conjugated fault patterns affecting the rigid body (i.e. SCB).

## 6. Discussion

The mentioned fault pattern undergoes reactivation in a new kinematic setting with two distinct tectonic regimes: one involving a closing zipper in the northeastern region and the other featuring a stretching junction in the northwestern Iranian plateau (Figure 5). In the eastern region, the fault pattern consists of a Y-shaped network of NNW- and NE-trending conjugated faults, incorporating a segment referred to as an extracted fault (see Figure 5). The NNW and NE fault groups have been the subject of detailed individual studies conducted by Shabanian et al. (2010) and Javidfakhr et al. (2011a, b) respectively.

Conversely, the fault system in the northwestern Iranian plateau (Figure 5b) presents a complex pattern characterized by the heightened activity and wide distribution of two sets of sinistral NE- and dextral NW-trending faults (Mokhoori et al., 2021; Hessami et al., 2003). The overall configuration of the fault pattern resembles a fishbone structure with the suture zone serving as the backbone (as depicted in Figure 2a). This suggested structure is notably prevalent in northeastern Iran, where the Kopeh Dagh and Binalud mountains are constrained and separated by the Turan and Lut rigid plates, firmly anchored by the suture zone (e.g., Hollingsworth et al., 2006). In each of the zippered system where the geometry of the faults changes, the stress state may also undergo some modifications. For example, on the Doruneh fault (DOF in Figure 1) in the frontal part of the Lut microplate and some segments of the suture zone in southeastern and southwestern of the SCB along the Alborz range (SHF in Figure 1), the stress state changes from transpressional to transtensional (e.g. Malekzade & Bellier, 2023, Hessami, 2020; this study). The change in stress state may alter the seismic pattern. In other words, the change in stress state may modify the fault kinematics and consequently alter the return period.

With a brief overview of historical and instrumental recorded events, it becomes apparent that some locations on maps lack a significant history of seismic events (see Figure 6a). Unfortunately, non-specialized researchers in tectonic studies (see Figure 6b, c) may incorrectly perceive aseismic areas or regions lacking surface fault exposure as having low seismic risk. However, as argued in this study, these areas could potentially be active seismic zones.

For example, in Figure 6a, certain highlighted areas on the map are designated as lower seismic hazard zones. Nevertheless, these areas are actually situated in the same tectonic zones and should be closely monitored as potential future seismic sources. It is recalled that the fatal M7.5 20 June 1990 Rudbar along the suture zone was not mapped previously.

## 7. Conclusion

Based on the points presented in this study, certain tectonic factors can lead to a more realistic hazard assessment program and an objective calculation of the return period for a significant event. This study aim to illustrate that the suture zone serves as a weak area for releasing accumulated strain, manifesting as aseismic creeping deformation or earthquakes in various forms. Additionally, the study seeks to elucidate the impact of the SCB on the deformation patterns of the surrounding regions. The westward movement of the SCB could alter the configuration of the seismic-prone suture zone, consequently affecting the seismic activity in the area.

Hence, the absence of seismic activity in a fault segment does not imply inactivity. Rather, it may signify the accumulation of strain or ongoing creeping deformation. Ultimately, the study endeavors to emphasize that the seismic hazard along the shear zones overlaying active faults remains constant. Nonetheless, it is evident that specific sections of the shear zones intersect densely populated areas, warranting heightened scrutiny. In essence, a seismic map tailored for hazard assessment should be distinguished from maps designed for seismic risk analysis.

## Acknowledgments

Author acknowledges to O. Bellier due to check the fault kinematics results.

## References

Afra, M., Moradi, A., & Pakzad, M. (2017). Stress regimes in the northwest of Iran from stress inversion of earthquake focal mechanisms. *Journal of Geodynamics*, *111*, 50-60.

Avagyan, A., Sosson, M., Philip, H., Karakhanian, A., Rolland, Y., Melkonyan, R., ... & Davtyan, V. (2005). Neogene to Quaternary stress field evolution in Lesser Caucasus and adjacent regions using fault kinematic analysis and volcanic cluster data. *Geodinamica Acta*, *18*(6), 401-416.

Azad, S. S., Nemati, M., Abbassi, M. R., Foroutan, M., Hessami, K., Dominguez, S., Bolourchi, M. J., & Shahpasandzadeh, M. (2019). Active-couple indentation in geodynamics of NNW Iran: Evidence from synchronous left- and right-lateral co-linear seismogenic faults in western Alborz and Iranian Azerbaijan domains. *Tectonophysics*, *754*, 1-17.

Bellier, O., & Zoback, M. (1995). Recent state of stress change in the Walker Lane zone western Basin and Range province, USA. *Tectonics*, *14*, 564-593. https://doi.org/10.1029/94TC00596

Berberian, M., & Walker, R. (2010). The Rudbar Mw 7.3 earthquake of 1990 June 20; seismotectonics, coseismic and geomorphic displacements, and historic earthquakes of the western 'High-Alborz', Iran. *Geophysical Journal International*, *182*, 1577-1602. https://doi.org/10.1111/j.1365-246X.2010.04705.x

Carey, E. (1979). Recherche des directions principales de contraintes associées au jeu d'une population de failles. *Revue de Géologie Dynamique et de Géographie Physique*, *21*(1), 57-66.

Carey, E., & Brunier, B. (1974). Analyse théorique et numérique d'un modèle mécanique élémentaire appliqué à l'étude d'une population de failles. *Comptes Rendus de l'Académie des Sciences de Paris, Série D*, *279*, 891-894.

Carey-Gailhardis, E., & Mercier, J.-L. (1987). A numerical method for determining the state of stress using focal mechanisms of earthquake populations: Application to Tibetan teleseisms and microseismicity of southern Peru. *Earth and Planetary Science Letters*, *82*(1-2), 165-179. https://doi.org/10.1016/0012-821X(87)90117-8.

Chu, Y., Allen, M.B., Wan, B., Chen, L., Lin, W., Talebian, M., Wu, L., Xin, G., & Feng, Z. (2021). Tectonic exhumation across the Talesh-Alborz Belt, Iran, and its implication to the Arabia-Eurasia convergence. *Earth-Science Reviews*, *221*, p.103776.Jack

Faccenna, C., Bellier, O., Martinod, J., Piromallo, C., & Regard, V. (2006). Slab detachment beneath eastern Anatolia: A possible cause for the formation of the North Anatolian fault. *Earth and Planetary Science Letters*, *242*(1-2), 85-97.

Farbod, Y., Bellier, O., Shabanian, E., & Abbassi, M. R. (2011). Geomorphic and structural variations along the Doruneh Fault System (central Iran). *Tectonics*, *30*, TC6014. https://doi.org/10.1029/2011TC002889

Hessami, K., Pantosi, D., Tabassi, H., Shabanian, E., Abbassi, M.-R., Feghhi, K., & Solaymani, S. (2003a).

Paleoearthquakes and slip rates of the North Tabriz fault, NW Iran: Preliminary results. *Annals of Geophysics*, *46*, 903-915.

Hessami, K. (2020). Polyphase inversion tectonics in western Alborz Mountains, northern Iran. *Iranian Journal of Geophysics*, *14*(4), 79-88.

Hollingsworth, J., Jackson, J., Walker, R., Reza Gheitanchi, M., & Javad Bolourchi, M. (2006). Strike-slip faulting, rotation, and along-strike elongation in the Kopeh Dagh Mountains, NE Iran. *Geophysical Journal International*, *166*(3), 1161-1177.

Jackson, J., Priestley, K., Allen, M., & Berberian, M. (2002). Active tectonics of the South Caspian Basin. *Geophysical Journal International*, *148*, 214-245.

Jackson, J., Bouchon, M., Fielding, E., Funning, G., Ghorashi, M., Hatzfeld, D., Nazari, H., Parsons, B., Priestley, K., Talebian, M., & Tatar, M. (2006). Seismotectonic, rupture process, and earthquake-hazard aspects of the 2003 December 26 Bam, Iran, earthquake. *Geophysical Journal International*, *166*(3), 1270-1292.

Javidfakhr, B., Bellier, O., Shabanian, E., Ahmadian, S., & Saidi, A. (2011a). Plio-Quaternary tectonic regime changes in the transition zone between Alborz and Kopeh Dagh mountain ranges (NE Iran). *Tectonophysics*, *506*, 86-108. https://doi.org/10.1016/j.tecto.2011.04.013

Javidfakhr, B., Bellier, O., Shabanian, E., Siame, L., Léanni, L., Bourlès, D., & Ahmadian, S. (2011b). Fault kinematics and active tectonics at the southeastern boundary of the eastern Alborz (Abr and Khij fault zones): Geodynamic implications for NNE Iran. *Journal of Geodynamics*, *52*(3-4), 290-303. https://doi.org/10.1016/j.jog.2011.02.005

Lyberis, N., & Manby, G. (1999). Oblique to orthogonal convergence across the Eurasia block in the post-Miocene. *AAPG Bulletin*, *83*(7), 1135-1154.

Malekzade, Z. (2018). Block rotation induced by the change from the collision to subduction: Implications for active deformations within the areas surrounding South Caspian Basin. *Mar. Geol.*, *404*, 111-129.

Malekzade, Z., & Bellier, O. (2023). The active changeover from the transpression to the transtensional tectonic regime in eastern Alborz, Northern Iran. *Journal of Asian Earth Sciences*, *246*, 105580.

Malekzade, Z., & Bellier, O. (2024). Tectonic model-based critique on conventional seismic hazard evaluations. *9th International Conference on Seismology and Earthquake Engineering*, Tehran, Iran.

Masson, F., Anvari, M., Djamour, Y., Walpersdorf, A., Tavakoli, F., Daignieres, M., et al. (2007). Large?scale velocity field and strain tensor in Iran inferred from GPS measurements: Newinsight for the present-day deformation pattern within NE Iran. *Geophysical Journal International*, *170*(1), 436-440. https://doi.org/10.1111/j.1365?246X.2007.03477.x

Masson, F., Djamour, Y., Van Gorp, S., Chéry, J., Tatar, M., Tavakoli, F., Nankali, H., & Vernant, P. (2006). Extension in NW Iran driven by the motion of the South Caspian Basin. *Earth and Planetary Science Letters*, *252*, 180-188.

Mokhoori, A. N., Rahimi, B., & Moayyed, M. (2021). Active tectonic stress field analysis in NW Iran-SE Turkey using earthquake focal mechanism data. *Turkish Journal of Earth Sciences*, *30*(2), 235-246.

Mousavi, Z., Walpersdorf, A., Walker, R. T., Tavakoli, F., Pathier, E., Nankali, H. R. E. A., Nilfouroushan, F., & Djamour, Y. (2013). Global Positioning System constraints on the active tectonics of NE Iran and the South Caspian region. *Earth and Planetary Science Letters*, 377, 287-298.

Nemati, M., Hatzfeld, D., Gheitanchi, M., Sadidkhouy, A., Mirzaei, N., & Moradi, A. (2011). Investigation of seismicity of the Astaneh Fault in the eastern Alborz. *Journal of the Earth and Space Physics*, *37*(2), 1-16.

Ritz, J.-F., Nazari, H., Salamati, R., Shafeii, A., Solaymani, S., & Vernant, P. (2006). Active transtension inside Central Alborz: A new insight into the Northern Iran-Southern Caspian geodynamics. *Geology*, *34*, 477-480.

Shabanian, E., Bellier, O., Abbassi, M. R., Siame, L., & Farbod, Y. (2010). Plio-Quaternary stress states in NE Iran: Kopeh Dagh and Allah Dagh-Binalud mountain ranges. Tectonophysics, 480, 280-304.

https://doi.org/10.1016/j.tecto.2009.10.022

Su, Z., Yang, Y.-H., Li, Y.-S., Xu, X.-W., Zhang, J., Zhou, X., Ren, J.-J., Wang, E.-C., Hu, J.-C., Zhang, S.-M., & Talebian, M. (2018). Coseismic displacement of the 5 April 2017 Mashhad earthquake (Mw 6.1) in NE Iran through Sentinel-1A TOPS data: New implications for the strain partitioning in the southern Binalud Mountains. *Journal of Asian Earth Sciences*, *169*, 244-256

Talebian, M., Fielding, E.J., Funning, G.J., Ghorashi, M., Jackson, J., Nazari, H., Parsons, B., Priestley, K., Rosen, P.A., Walker, R. and Wright, T.J. (2004). The 2003 Bam (Iran) earthquake: Rupture of a blind strike-slip fault. *Geophysical Research Letters*, *31*(11).

Tatar, M., & Hatzfeld, D. (2009). Microseismic evidence of slip partitioning for the Rudbar-Tarom earthquake (Ms 7.7) of 1990 June 20 in NW Iran. *Geophysical Journal International*, *176*(2), 529-541.

Tavakoli, B., & Ghafory-Ashtiany, M. (1999). Seismic hazard assessment of Iran. *Annals of Geophysics*, *42*(6).

Tavakoli, F. (2007). *Present-Day Kinematics of the Zagros and East of Iran Faults.* Ph.D. Thesis, University of Joseph Fourier. http://tel.archives-ouvertes.fr/tel-00285919/fr/

Zare, M. (2017). Seismic hazard zoning in Iran: A state-of-the-art on the studies during four decades. *Journal of Seismology and Earthquake Engineering*, *19*(2), 71-101.